J. Fluid Mech. (1979), *vol.* 90, *part* 3, *pp.* 415–431
Printed in Great Britain

The effects of certain low frequency phenomena on the calibration of hot wires

By A. E. PERRY, A. J. SMITS AND M. S. CHONG

Department of Mechanical Engineering, University of Melbourne,
Parkville, Victoria 3052, Australia

(Received 7 February 1977 and in revised form 16 May 1978)

Temperature-sensitive constant-current wires operating at very low resistance ratios have been tested for temperature fluctuation response. A significant step in the response was found to occur with a centre-frequency of typically $\frac{1}{6}$ Hz. The step size was observed to be as large as 30 % and grew from zero to its maximum value in about a decade. Analysis shows that this phenomenon is associated with axial conduction of heat to and from the prongs. If it is recognized that prongs have finite thermal inertia then a modification of the boundary conditions to the equations of Betchov (1948) predicts this step, in agreement with the simple asymptotic analysis of Maye (1970).

Experiments indicate that a similar phenomenon occurs with velocity-sensitive wires. Axial conduction appears to be the most likely cause. Aeroelastic deflexions and non-uniform cooling caused by bowing of the wire make precise predictions impossible. Here the differences in step size between wires were observed to be as large as 10 % (or 20 % in mean-square energy), the centre-frequency was usually beyond 10 Hz for the wires tested and the step extended over a much broader frequency range than in the temperature-sensitive case. The effect occurred at all velocities, resistance ratios and wire geometries. An analysis based on non-uniform cooling of the wire filament predicts the correct frequency range and shows that steps of 10 % in frequency response are quite plausible.

1. Introduction

The small diameter filament of a hot-wire probe generally has its ends coated with a cylindrical metallic layer, forming 'stubs' which are in turn connected to the probe prongs. When Wollaston wire is used, the filament is made from platinum and the stub is made from silver.

In the past, it has been assumed in analyses that the wire–stub junction is at the ambient temperature. But Champagne, Sleicher & Wehrmann (1967) found experimentally that at high resistance ratios the temperature at the ends of the wire was considerably above ambient. Thus the heat-transfer properties of the support were demonstrably influencing the wire heat transfer, and the dynamic response of the probe should include not only a wire thermal-inertia time constant but also time constants associated with the stub and prongs.

A hot wire is generally used in two distinct modes. To measure velocity fluctuations the wire is kept at a constant temperature and operated with a high resistance ratio,

while to measure temperature fluctuations the wire is run with a constant current at a very low resistance ratio.

In the case of temperature-fluctuation measurements it is found that the comparatively massive prongs have a dominant influence on the time constant of the end conduction phenomenon and the problem can be conveniently divided into a fast response system (the wire) and a slow response system (the prongs). The analysis then predicts a step in the system's frequency response at low frequencies, which gives a discrepancy between the static and dynamic sensitivities, as first suspected by Maye (1970) from a simple asymptotic analysis.

In the analysis presented here, the full transfer function is derived and shows over what frequency range the phenomenon occurs. A detailed comparison with experiment is presented for a family of wires. The theory and experiments show that the step can vary from 30% for a length-to-diameter ratio l/d of 100 to less than 2% for $l/d = 1000$ and that the centre-frequency of the step is about $\frac{1}{6}$ Hz for the probes used. Unless appropriate precautions are taken this can lead to large errors in the sensitivity calibration.

In the case of velocity-fluctuation measurements the problems are far more complex. Analysis shows that asymmetrical temperature distributions caused by wire bowing and aeroelastic deflexions result in an effective lowering of the wire time constant. At low frequencies the thermal inertia of the stub is important but not that of the prong. Furthermore, the lowering of the wire time constant means that the thermal inertia of both the stub and wire control the phenomenon and a convenient separation into two systems cannot be made.

Because of the complexity of the problem and the large array of variables beyond any control, a precise prediction by analysis and comparison with experiment is impossible. However, some aspects of the problem can be calculated and show that appreciable discrepancies between static and dynamic response are possible. This conforms with experiment.

2. Constant-current method for the measurement of temperature fluctuations

2.1. *Analysis*

Figure 1 defines some of the symbols and shows a wire and wire element. A heat balance on the element leads to the general time- and space-dependent relation

$$\frac{\partial^2\theta}{\partial x^2} - (\xi - q)\,\theta - \tau\frac{\partial(\theta+\theta_g)}{\partial t} = \frac{-q}{\alpha}. \tag{1}$$

Here θ is the local temperature along the wire measured relative to the instantaneous gas temperature θ_g, which is uniform in space but varies with time and is measured relative to some fixed datum. The co-ordinate x has been non-dimensionalized by the wire length l. The quantities ξ and q denote $h\pi dl^2/kA$ and $I^2R_g\alpha l/kA$ respectively, where I is the wire current, R_g is the wire resistance at the instantaneous gas temperature, h is the wire film coefficient, α is the temperature coefficient of resistivity of the wire material and k is its thermal conductivity. The constant τ denotes $\rho cl^2/k$, where ρ is the wire density and c is its specific heat. The velocity of flow over the wire is assumed to be constant and hence ξ is constant.

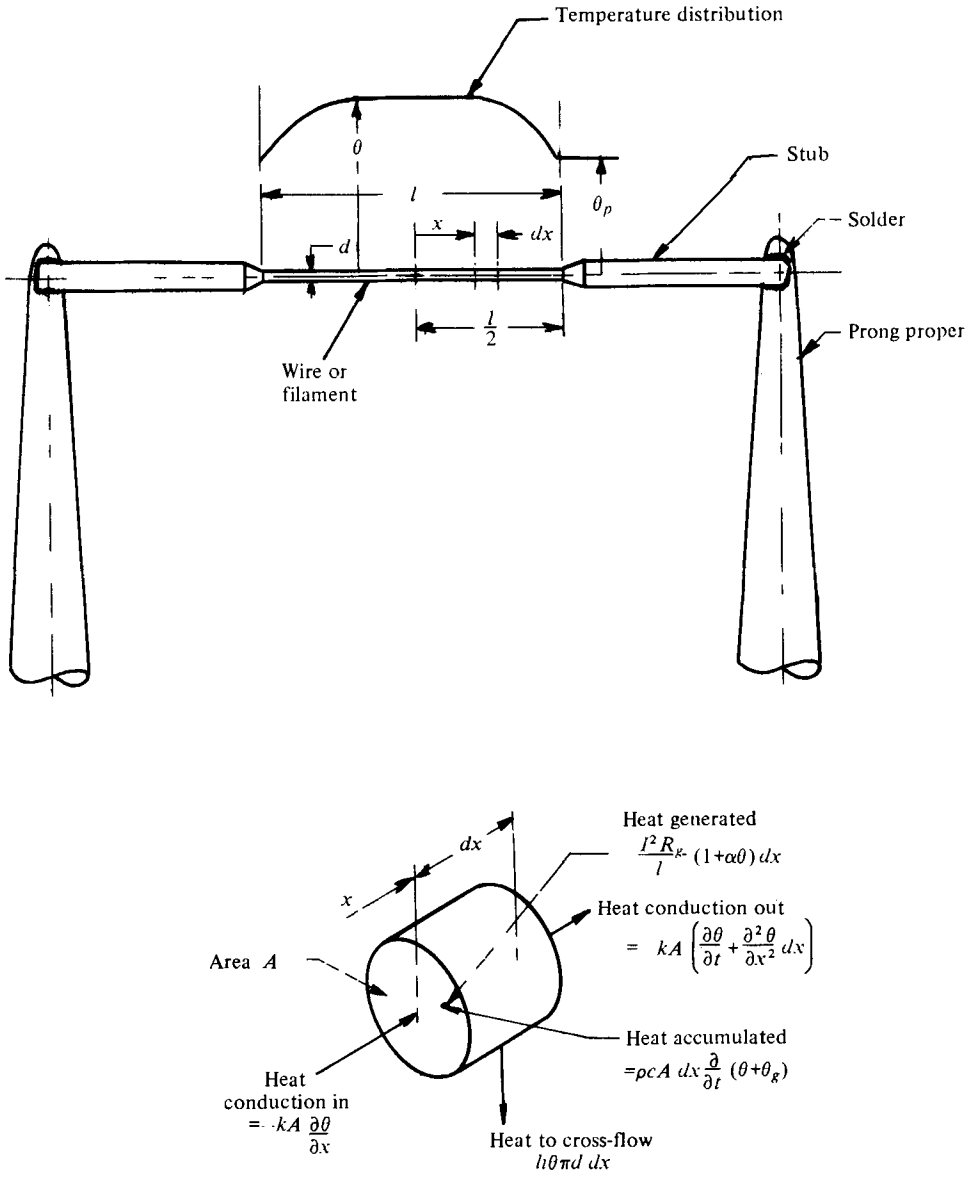

FIGURE 1. Hot-wire geometry and definition of quantities.

Boundary conditions must be applied to (1), and these must come from a consideration of the prongs. As the temperature of the gas varies, the entire prong and stub system must be heated and cooled and the heat flow must occur via the boundary layers surrounding the prong and stub. For simplicity the prong will be 'lumped', i.e. regarded as being made up of discrete components as indicated by the electrical analogue circuit shown in figure 2.

For the purpose of this exercise, imagine that the prong is connected to an infinite heat sink where it adjoins the probe holder and that the temperature of this sink is at the mean gas temperature.

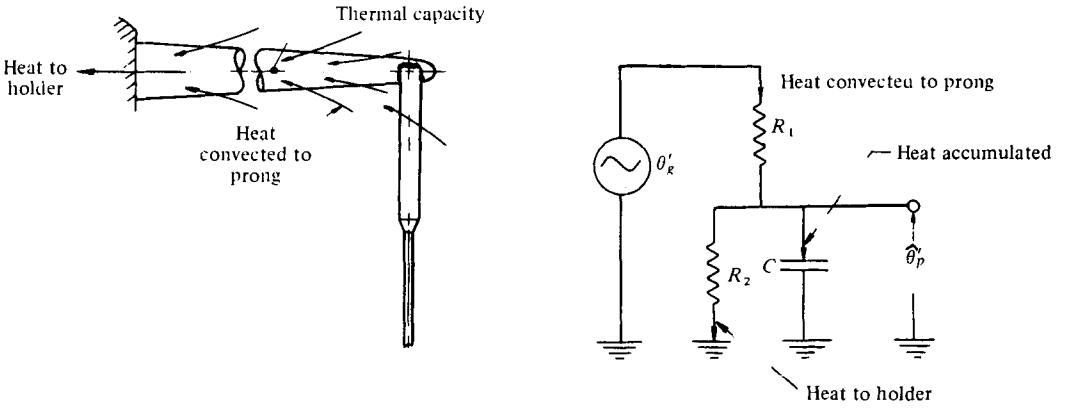

FIGURE 2. Simple analogue for prong heat balance.

Let θ'_g be the perturbation in gas temperature and let $\hat{\theta}'_p$ be the perturbation in prong temperature, both measured relative to a fixed datum. The prong will be heated up by heat flow through the boundary layer on its surface, which has a thermal resistance R_1. Some of this heat will accumulate in the thermal capacitor C and some will be conducted down the prong to the infinite sink through the resistance R_2. Because of the massiveness of the prong, the amount of heat flowing to the wire filament will have a negligible effect on the thermal balance of the prong. Hence $\hat{\theta}'_p$ becomes a forcing function for the wire filament and is determined by the prong and external flow conditions.

The transfer function for the prong in Laplace-transform form is

$$\hat{\theta}'_p/\theta'_g = G/(1+T_p s), \tag{2}$$

where $G = R_2/(R_2+R_1)$ and $T_p = GR_1C$. One would expect G to be of order one since under sufficiently slowly varying conditions $\hat{\theta}'_p \approx \theta'_g$. The quantity s is the Laplace variable and for steady-state response to sinusoidal perturbation $s = i\omega$, where $i = \sqrt{-1}$. Overbars denote a temporal mean.

A time-dependent solution of (1) shows that the characteristic time constant T_w for the wire is τ/Π, where $\Pi = \xi - q$ (Betchov 1948), and this is typically 0·001 s. This is the usual 'bulk heating' time constant associated with filaments. Hence at low frequencies one can regard the filament as responding instantly to fluctuations in gas temperature and the time-derivative term can be dropped.

Assume symmetry conditions and let

$$2\int_0^{\frac{1}{2}} \theta\, dx = \langle\theta\rangle.$$

A solution for θ_p can then be obtained from (1). Noting that $\theta_p = \hat{\theta}_p - \theta_g$, this solution can be combined with (2) to give a relationship between $\langle\theta\rangle$ and θ_g. From the definition of α, $\langle\theta\rangle = (R_w - R_g)/\alpha R_g$, where R_w is the wire resistance. A linearized perturbation equation can then be derived which gives the transfer function between r_w and r_g, the perturbation resistances. Let the resistance ratio R $(=\bar{R}_w/R_g)$ approach unity.

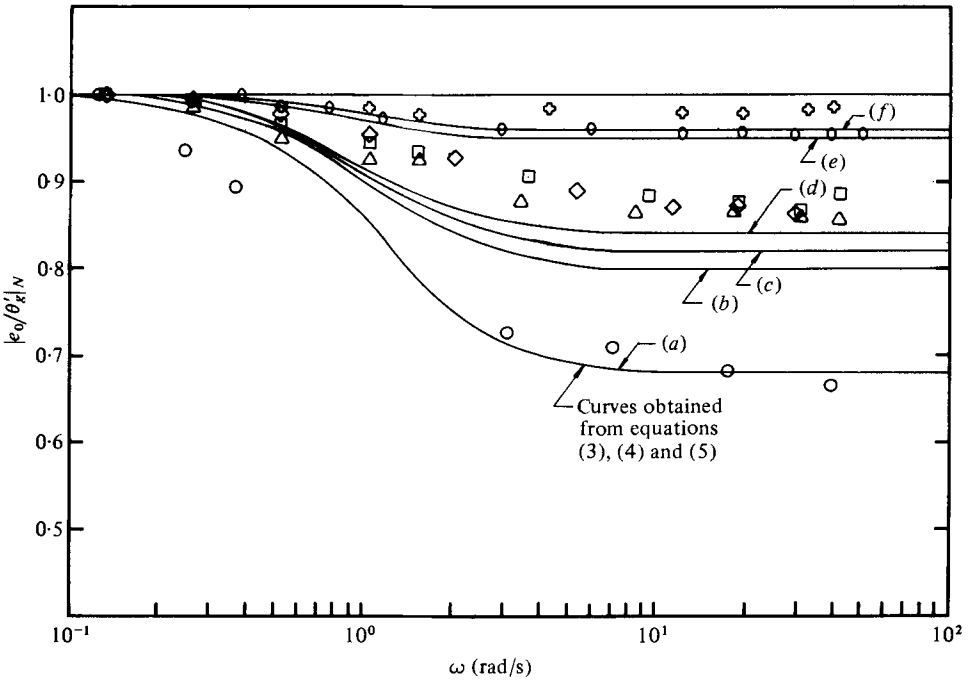

FIGURE 3. Response of wires to gas-temperature fluctuations.

		d	l	U			d	l	U
(*a*)	○	5 μm	0·5 mm	11·5 m s^{-1}	(*d*)	◇	5 μm	0·9 mm	20·5 m s^{-1}
(*b*)	△	5 μm	0·9 mm	5·5 m s^{-1}	(*e*)	⬯	3 μm	2 mm	11·5 m s^{-1}
(*c*)	□	5 μm	0·9 mm	11·5 m s^{-1}	(*f*)	✣	1 μm	1 mm	11·5 m s^{-1}

The quantity $\bar{q}$ then approaches zero and after a considerable amount of algebra and binomial expansions one obtains

$$\left(\frac{r_w}{r_g}\right)_N = \left(\frac{e_0}{\theta'_g}\right)_N = \left[\frac{1+(1+\epsilon)T_p s}{1+T_p s}\right], \tag{3}$$

where ϵ is a small quantity given by

$$\epsilon = -2G/\xi^{\frac{1}{2}}. \tag{4}$$

Overbars denote temporal means, e_0 is the voltage perturbation across the wire and the suffix N denotes that the transfer function has been normalized to be unity at zero frequency. With $s = i\omega$, the modulus of $(e_0/\theta'_g)_N$ has a step in frequency response with a centre-frequency $\omega_c = 1/T_p$.

Maye (1970) arrived at (4) (with $G = 1$) by assuming that at high frequencies the prongs were at the temporal mean gas temperature. He was not concerned with the frequency dependence as given by (3).

2.2. *Temperature-fluctuation experiments*

Accurately known sinusoidal perturbations in temperature are difficult to produce. However, square waves were produced by slowly oscillating the wire across two adjacent streams of the same velocity with one stream at an elevated temperature

relative to the other. The two streams were separated by a splitter plate and the wire was located downstream of its trailing edge. A constant-current anemometer operating with platinum Wollaston wire soldered onto a DISA 55F14 prong was used with a resistance ratio of typically 1·01. The velocity sensitivity of the wire was negligible.

Figure 3 shows a Bode diagram for a number of different wires with gas temperature perturbations and operating under a number of different flow conditions. These results have been compared with the theoretical predictions of (3) and (4).

The value of G was estimated by applying a simple empirical heat-transfer formula to the prong to calculate R_1, and R_2 can be calculated using the Fourier heat-conduction formula. The stub was ignored. This gave G 0·7. T_p can be estimated similarly and this gave $T_p \approx 1{\cdot}4$ s. Experiments indicate $T_p \approx 1$ s. It can be shown that

$$\epsilon = -GNu^{-\frac{1}{2}} \left(\frac{k}{k_a}\right)^{\frac{1}{2}} \left(\frac{d}{l}\right), \tag{5}$$

where Nu is the Nusselt number of the wire and k_a is the thermal conductivity of air. From Hinze (1959), for air at normal temperature and pressure $Nu \simeq 0{\cdot}39 + 0{\cdot}51Re^{\frac{1}{2}}$, where Re is the Reynolds number of the wire. For the purpose of prediction a safe and conservative value of G is unity.

Figure 3 indicates that substantial errors can occur if wires are calibrated statically and then used in a dynamic situation. These errors are reduced as the length-to-diameter ratio increases. The data agree reasonably well with (3), and also the predictions of Maye (1970) for ϵ have now been confirmed experimentally.

3. Constant-temperature hot wire for velocity-fluctuation measurements

3.1. *Experiments with velocity fluctuations*

Many preliminary experiments carried out by the authors indicate that a similar step in frequency response occurs in the case of velocity-fluctuation measurements but that the characteristic frequency is higher and the frequency range much broader than in the temperature-fluctuation case. Measurements of absolute values of the step size ϵ are most difficult. Perry & Morrison (1971*a*) managed to obtain frequency response curves for constant-temperature wires using a low frequency shaker in the range 1–15 Hz and a Kármán vortex-shedding technique for the range 500 Hz–10 kHz. The response was found to be flat in these ranges. Measurements by these methods become impractical in the important range 15 Hz–1 kHz. Also the vortex-shedding method cannot produce a response curve for a fixed mean velocity. An attempt was made by Perry & Morrison (1972) to bridge this frequency gap by using a vibrating table. The wire was oscillated sinusoidally in a uniform steady stream and the hot-wire output was compared with the integrated output from an accelerometer mounted on the table. Both signals were passed in turn through the same notch filter to remove spurious harmonics. It can be seen from figure 4 that a step in the response does occur but the hot-wire filament undergoes a mechanical resonance. Its motion then no longer conforms with that of the table. Thus it could be argued that the inertia forces which are present cause the filament to undergo unnatural motions even before resonance. Thus the experiment does not faithfully simulate a stationary wire in a fluctuating stream.

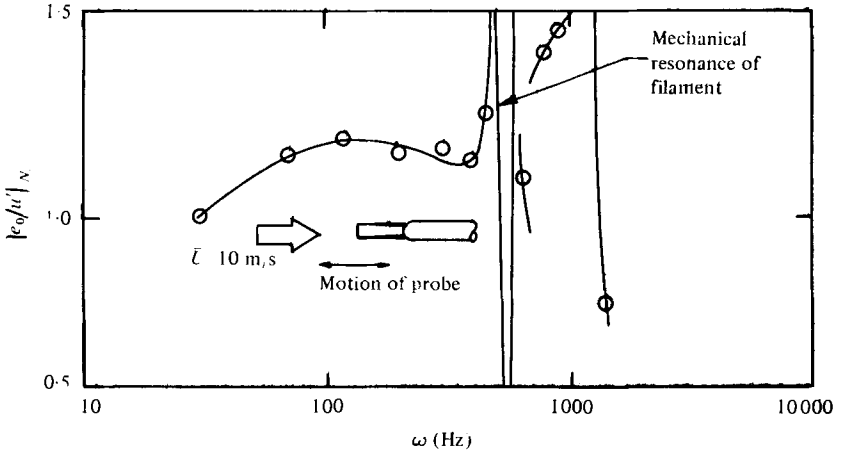

FIGURE 4. Hot-wire response to forced oscillation in steady flow. Mechanical resonance unusually low in this case. Normalized at $\omega = 30$ Hz. (After Perry & Morrison 1972.)

Another method for determining ϵ would be to put the wire in a 'known' flow with a large spread of frequency components in the velocity fluctuations. To know the flow, one must measure it with another instrument at the same time. A laser-Doppler system would be ideal but the necessary seeding would affect the hot-wire performance.

Thus at present the authors see no definitive way of measuring absolute values of ϵ. The best that can be done is to use another hot wire and make comparison tests. Thus arbitrary wire pairs were chosen and the differences in their ϵ's were measured. Let this difference be $\Delta\epsilon$ for a given wire pair.

A variety of double probes were so constructed that the pair of wire filaments were parallel and no more than about one wire filament length apart. These were mounted with their filaments horizontal downstream of a turbulence-producing grid set across the entrance of the working section of the tunnel. The grid consisted of horizontal strips. To ensure that sufficient turbulent energy was present at low frequency, a vertical oscillating flap was placed in the flow upstream and to one side of the hot-wire probes. This increased the rate of convergence of the data sampling at the low-frequency settings. Turbulence intensities were typically 5 % and the mean velocity 10 m/s. The wire properties are given in the figures.

Bode diagrams for $\Delta\epsilon$ were determined by processing the signals from the two hot-wire channels simultaneously using two sets of notch filters (one octave wide) and two sets of squaring circuits and analog integrators. An EAI TR48 analog computer was used. The integration times were 90 s and were repeated until the variance of the accumulated mean squares was less than $\frac{1}{2}$ %. The two processing channels were calibrated for any mismatch in frequency response at all frequency settings to an accuracy of 0·1 %. This was done by passing the same hot-wire signal into both channels simultaneously. All results were corrected for noise and any d.c. offsets. The hot-wire sets had frequency responses well beyond 20 kHz.

Let the two hot-wire channels be A and B and the r.m.s. voltages be e_A and e_B. A normalized Bode curve could be written as

$$(e_A/e_B)_N = 1 + \Delta\epsilon f(\omega), \tag{6}$$

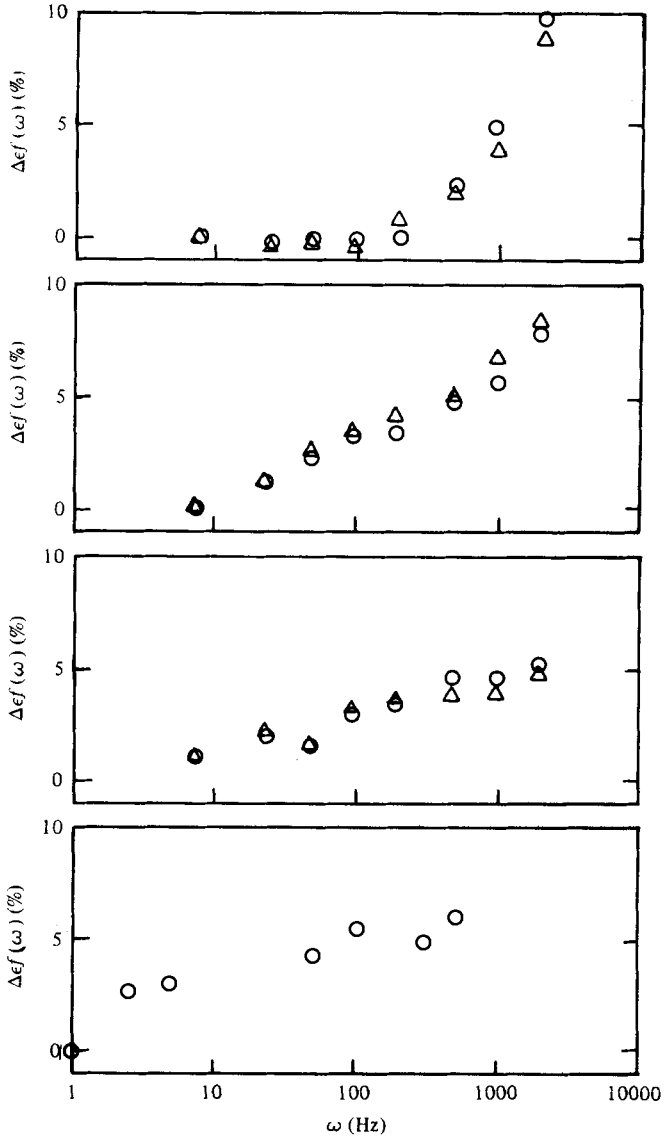

FIGURE 5. Experimental Bode plots. Each figure is for a given wire pair. Wires in a given pair were interchanged, giving two plots. ○, $\Delta\epsilon$ positive; △, $\Delta\epsilon$ negative. Platinum Wollaston wire 5 μm diameter, $R = 1{\cdot}5$, $\bar{U} = 10$ m/s used throughout. (*a*), (*b*) DISA type 55F14 geometry, i.e. 3 mm between prongs, and $l/d = 200$. (*c*), (*d*) 5 mm between prongs, $l/d = 400$. No reflexion test carried out for case (*d*).

where $f(\omega)$ has the properties $f(0) = 0$ and $f(\infty) = 1$. Figures 5(*a*)–(*d*) show four typical Bode diagrams for $\Delta\epsilon f(\omega)$ where $(e_A/e_B)_N$ has been normalized to unity at low frequency.

To ensure that the phenomenon was not due to any spurious electronic effects, probe A was unplugged and connected to anemometer B and its associated computing channel and vice versa for probe B. Hence in this second test

$$(e_A/e_B)_N = 1 - \Delta\epsilon f(\omega). \tag{7}$$

That is, $\Delta\epsilon$ should effectively change sign and the Bode diagram should be reflected.† This reflexion is seen to occur with high accuracy. Thus the phenomenon has been isolated to the hot-wire filament, probe and cable. By using the same probes and cables with different hot wires, it was found that the effect was characteristic of the filaments.

To ensure that no anomaly in the flow position was causing the effect, the two wires were slowly traversed across the flow vertically and sinusoidally through a distance of 3 in. at about $\frac{1}{2}$ Hz while the data were being taken.

It can be seen that the values of $\Delta\epsilon$ are significant and that a variety of $\Delta\epsilon f(\omega)$ distributions are possible. Other tests which compared broad-band turbulence with low frequency sinusoids using the dynamic calibrator developed by Perry & Morrison (1971*a*) yielded on occasions discrepancies of approximately 10 %. These tests would considerably underestimate $\Delta\epsilon$. Again reflexion tests were carried out. With the aid of these experiments and many others like it, the authors conclude that there is no simple or obvious property of the wires which can be related to $\Delta\epsilon$. Further detailed observations in the next subsection explain how complex this problem is.

3.2. *Modelling the problem*

Consider a constant-temperature flow with fluctuating velocity. The only source of heat supplied to the prong is from the wire. Assuming the prong to be massive, the stub will be the only element of the support system at an elevated temperature and will be heated at one end. Thus a distributed rather than a lumped system must be used, with heat waves travelling down the stub from the wire.

Some important experimental observations must be discussed before sensible modelling can begin. When measuring velocity fluctuations wires are usually run hot at a resistance ratio R of 1·5–2. As reported by Perry & Morrison (1971*b*, 1972) and Perry (1972), wires bow under the action of thermal expansion and become buckled columns, even when they are initially straight. They have a very low elastic resistance to lateral aerodynamic loads, and the bow rotates about an axis through the stubs as the air velocity is increased. This bow is responsible for the mechanical resonance noted earlier in figure 4.

The phenomenon is highly nonlinear and in some cases the wire will 'flip over' once a critical velocity is reached. In other cases the bow orientation varies gradually with velocity. Bows appear to have a marked effect on the temperature distribution along the wire. By running wires at a resistance ratio of about 2·5 in a flow and viewing them under a microscope the point of maximum temperature shows up as a hot spot; see figure 6 (plate 1). For a slightly asymmetrical bow, the hot spot moves towards the stub as the bow rotates, and sometimes the hot spot will settle near a kink.

There could be many causes for this. Wire-property variations associated with stress variations, surface contamination or axial flow components along the wire induced by the wire bow are some possible explanations for perturbations in the symmetry of the temperature distribution.

Even the spatial mean effective film coefficient can be affected by the orientation of the bow. This was demonstrated by placing a wire in a fixed uniform flow and rotating

† This 'reflexion' test is crucial. It is a stringent test of all aspects of the experiment and equipment (and hot-wire operator).

the bow by means of an externally applied magnetic field. Thus as the velocity of flow fluctuates, the orientation of the bow fluctuates, causing the distribution of the effective film coefficient to fluctuate. The bow will faithfully and consistently follow the velocity fluctuations up to the mechanical response frequency, typically 1–2 kHz (Perry & Morrison 1972).

There are many directions one could take in formulating an analysis. The authors offer a first attempt at the problem in § 4. There the phenomenon is modelled by a perturbation in the symmetry of the film coefficient. Future studies should investigate other possibilities when the physics are better understood. An important feature of this preliminary analysis is that, since the temperature distribution is asymmetrical, the assumption that the wire time constant T_w is τ/Π will not be valid and in fact it is found that the thermal effects within the wire itself can extend their influence down to the low characteristic frequency of the stubs.

The analysis indicates the frequency range over which the end-conduction effects occur, and this agrees with the experimental results for $\Delta\epsilon$. The complexity of the problem is obvious and, beyond demonstrating that large ϵ's are possible, detailed comparison between experiment and theory cannot be made. This would require knowledge of a number of aeroelastic derivatives which are peculiar to any given wire.

4. Analysis of velocity-sensitive constant-temperature wire response

4.1. *Basic equations*

Equation (1) will be non-dimensionalized by $\langle\theta\rangle$ to give

$$\frac{\partial^2\theta}{\partial x^2} - (\xi(x) - q)\,\theta - \tau\frac{\partial\theta}{\partial t} = -\frac{q}{Z}. \tag{8}$$

This equation is valid for a steady gas temperature and constant $\langle\theta\rangle$. $Z = R - 1$. It will be noted that ξ, the film coefficient parameter, is a function of x.

Taking a time average for small perturbations about a mean gives a static equation

$$\frac{d^2\bar{\theta}(x)}{dx^2} - (\bar{\xi}(x) - \bar{q})\,\bar{\theta}(x) = -\frac{\bar{q}}{Z} \tag{9}$$

with the following boundary and normalizing conditions:

$$\left(\frac{d\bar{\theta}}{dx}\right)_{-\frac{1}{2}} = \bar{\theta}_{-\frac{1}{2}} K_0, \quad \left(\frac{d\bar{\theta}}{dx}\right)_{\frac{1}{2}} = -\bar{\theta}_{\frac{1}{2}} K_0, \quad \int_{-\frac{1}{2}}^{\frac{1}{2}} \bar{\theta}\,dx = 1. \tag{10a–c}$$

Here $K_0 = Hl/kA$, which is a non-dimensional overall heat-transfer coefficient of the stub. H is the heat flow per unit time to the stub from the wire per unit temperature θ_p at the wire–stub junction.

By considering small perturbations about a temporal mean and linearizing for time variations, (8) gives

$$\frac{d^2\theta'}{dx^2} - (\bar{\xi}(x) - \bar{q} + \tau s)\,\theta'(x) = \xi'(x)\,\bar{\theta}(x) - q'\bar{\theta}(x) - \frac{q'}{Z} \tag{11}$$

with the boundary conditions

$$\left(\frac{d\theta'}{dx}\right)_{-\frac{1}{2}} = \theta'_{-\frac{1}{2}} K(s), \quad \left(\frac{d\theta'}{dx}\right)_{\frac{1}{2}} = -\theta'_{\frac{1}{2}} K(s), \quad \int_{-\frac{1}{2}}^{\frac{1}{2}} \theta'\,dx = 0. \tag{12a–c}$$

Here primes denote perturbations and overbars a temporal mean. Equation (12*c*) is a result of the feedback circuit which maintains a constant spatial-average temperature. $K(s)$ is a frequency-dependent overall heat-transfer coefficient of the stub.

One end of the stub is connected to a massive prong which will be assumed to be at the steady gas temperature. The other end of the stub is at a temperature $\theta_p = \theta_{+\frac{1}{2}}$ or $\theta_{-\frac{1}{2}}$. Treating the stub as a cylinder and neglecting cross-flow cooling and heat generation (both of which can be shown to be small) leads to a greatly simplified version of (8) which can then be applied to the stub. This leads to a solution for $K(s)$ given by

$$K(s) = K_0(\tau_s s)^{\frac{1}{2}} \coth{(\tau_s s)^{\frac{1}{2}}}, \tag{13}$$

where

$$\tau_s = \rho_s C_s l_s^2 / k_s. \tag{14}$$

This is the characteristic time constant of the stub and is usually of the order of 0·03 s. The suffix s denotes stub properties.

Consider the distribution of $\bar{\xi}(x)$. Because (9) and (11) are nonlinear in x, the distribution was so chosen that the equations were piecewise linear. Figure 7 illustrates this. Equations (9) and (11) must now be solved in the two regions 1 and 2 shown in the figure. Additional boundary conditions must be added to ensure matching of temperatures and temperature gradients at the junction defined by $x = \lambda$.

4.2. *Aeroelastic effects and the step ϵ in the frequency response*

To calculate the step in the frequency response it is necessary to evaluate dq/dU at zero frequency and at infinite frequency. At infinite frequency, the temperature distribution along the wire will cease to vary with time. The error or step is then

$$\epsilon = \left(\frac{dq}{dU}\right)_\infty \Big/ \left(\frac{dq}{dU}\right)_0 - 1. \tag{15}$$

This step also applies for the normalized transfer function $(e_0/u')_N$, where e_0 is the voltage fluctuation and u' is the velocity fluctuation.

In an actual flow, as the velocity fluctuates λ, n and ξ_1 will all simultaneously fluctuate owing to the aeroelastic behaviour of the filament. Hence

$$\frac{dq}{d\bar{U}} = \frac{\partial q}{\partial \lambda}\frac{d\lambda}{d\bar{U}} + \frac{\partial q}{\partial n}\frac{dn}{d\bar{U}} + \frac{\partial q}{\partial \xi_1}\frac{d\xi_1}{d\bar{U}}. \tag{16}$$

Following through this analysis, it is simple to show that ϵ has three contributions, i.e.

$$\epsilon = W_\lambda \epsilon_\lambda + W_n \epsilon_n + W_{\xi_1} \epsilon_{\xi_1}, \tag{17}$$

where

$$\epsilon_\lambda = \left(\frac{\partial q}{\partial \lambda}\right)_\infty \Big/ \left(\frac{\partial q}{\partial \lambda}\right)_0 - 1, \quad \epsilon_n = \left(\frac{\partial q}{\partial n}\right)_\infty \Big/ \left(\frac{\partial q}{\partial n}\right)_0 - 1, \quad \epsilon_{\xi_1} = \left(\frac{\partial q}{\partial \xi_1}\right)_\infty \Big/ \left(\frac{\partial q}{\partial \xi_1}\right)_0 - 1, \tag{18}$$

$$W_\lambda = \frac{1}{\Sigma}\left(\frac{\partial q}{\partial \lambda}\right)_0 \frac{d\lambda}{d\bar{U}}, \quad W_n = \frac{1}{\Sigma}\left(\frac{\partial q}{\partial n}\right)_0 \frac{dn}{d\bar{U}}, \quad W_{\xi_1} = \frac{1}{\Sigma}\left(\frac{\partial q}{\partial \xi_1}\right)_0 \frac{d\xi_1}{d\bar{U}} \tag{19}$$

and

$$\Sigma = \left(\frac{\partial q}{\partial \lambda}\right)_0 \frac{d\lambda}{d\bar{U}} + \left(\frac{\partial q}{\partial n}\right)_0 \frac{dn}{d\bar{U}} + \left(\frac{\partial q}{\partial \xi_1}\right)_0 \frac{d\xi_1}{d\bar{U}}. \tag{20}$$

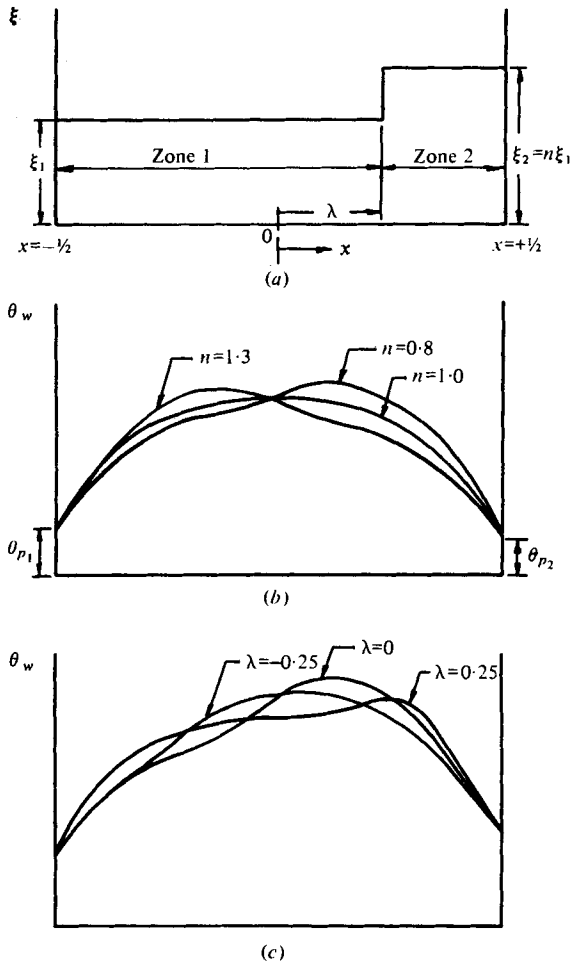

FIGURE 7. Definition of quantities and temperature distribution. (*a*) Definition of quantities. (*b*), (*c*) Typical computed temperature distributions; $d = 5\,\mu$m; $l/d = 100$; $\bar{U} = 10$ m/s, giving $\xi_1 = 72$, $l_s/l = 2{\cdot}95$; $d_s/d = 5$, giving $K_0 = 50$; $R = 1{\cdot}5$. (*b*) Different values of n ($\lambda = 0$). (*c*) Different values of λ ($n = 0{\cdot}5$).

W_λ, W_n and W_{ξ_1} are weighting factors which must sum to unity. Their values are dependent on how λ, n and ξ_1 vary with U. This information can come only from a detailed knowledge of the aeroelastic behaviour of the wire and how the distribution of ξ is affected by the wire orientation. Thus it can be seen that it is well-nigh impossible to make any precise predictions in a given situation. All that can be done is to give an idea of the potential errors by examining the values of e_λ, e_n and e_{ξ_1}, which fortunately can be calculated.

Equation (9) yields a set of solutions as follows:

$$\bar{\theta}_1 \equiv \bar{\theta}_1(Z, \xi_1, \lambda, n, K_0, x, \bar{q}), \tag{21}$$

$$\bar{\theta}_2 \equiv \bar{\theta}_2(Z, \xi_1, \lambda, n, K_0, x, \bar{q}). \tag{22}$$

By integrating (21) and (22) with respect to x and noting the normalizing conditions given by (10), we obtain

$$\bar{q} \equiv \bar{q}(Z, \xi_1, \lambda, n, K_0). \tag{23}$$

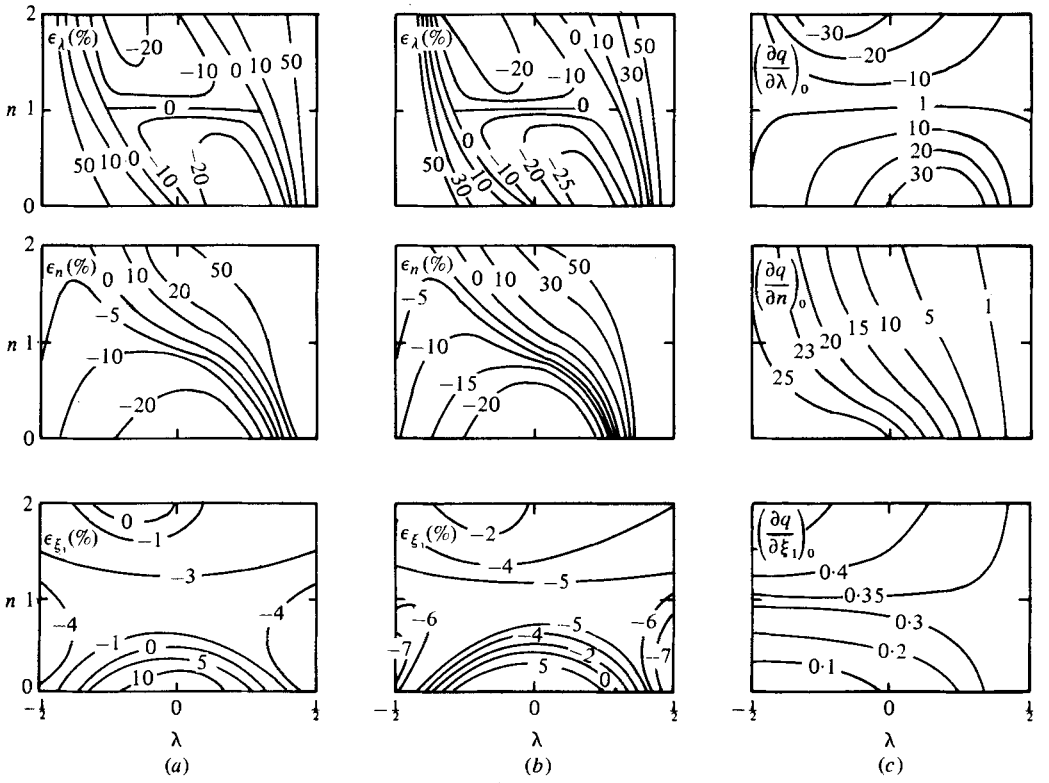

FIGURE 8. (*a*) Contours of ϵ_λ, ϵ_n and ϵ_{ξ_1} on the λ, n plane for $K = 30$. (*b*) Same for $K = 100$. (*c*) Contours of $(\partial q/\partial\lambda)_0$, $(\partial q/\partial n)_0$ and $(\partial q/\partial\xi_1)_0$ on the λ, n plane for $K = 30$. $\xi_1 = 72$ and $R = 1{\cdot}5$ throughout.

This turns out to be a non-explicit expression for $\bar{q}$ which is solved by iteration once Z, ξ_1, λ, n and K_0 are specified.†

By numerical perturbations about a chosen operating point the derivatives $(\partial n/\partial\lambda)_0$, $(\partial q/\partial n)_0$ and $(\partial n/\partial\xi_1)_0$ can be determined.

Consider (11). At infinite frequency $\theta'(x)$ must approach zero. Integrating (11) and noting that

$$\int_{-\frac{1}{2}}^{\frac{1}{2}} \tau s\theta' dx = 0,$$

one obtains

$$q' = \frac{Z}{Z+1}\int_{-\frac{1}{2}}^{\frac{1}{2}} \xi'(x)\,\bar{\theta}(x)\,dx. \tag{24}$$

From (21) and (22), $\bar{\theta}(x)$ is found. If it is known how $\xi'(x)$ depends on the perturbations λ', n' and ξ_1', (24) gives the derivatives $(\partial q/\partial\lambda)_\infty$, $(\partial q/\partial n)_\infty$ and $(\partial q/\partial\xi_1)_\infty$. Hence ϵ_λ, ϵ_n and ϵ_{ξ_1} can be found and these are mapped out in figure 8 for two values of K_0 (30 and 100). From the Fourier conduction formula applied to the stub

$$K_0 \simeq \frac{l}{l_s}\frac{k_s}{k}\left(\frac{d_s}{d}\right)^2. \tag{25}$$

† A copy of the rather lengthy expressions for $\bar{\theta}_1$, $\bar{\theta}_2$ and $\bar{q}$ can be obtained from the authors or from the Editor.

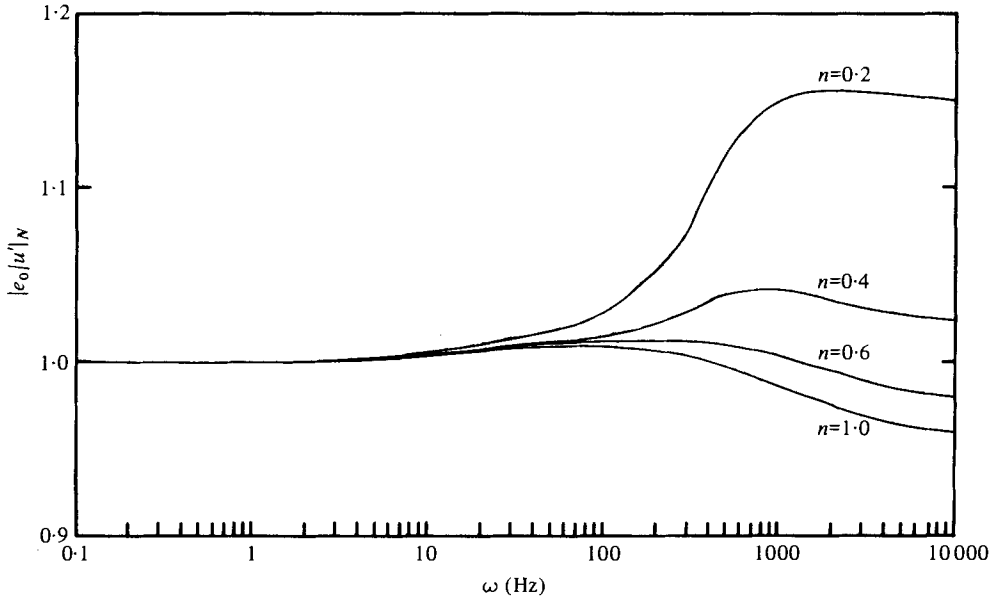

FIGURE 9. Theoretical Bode plots for perturbations in ξ_1 for fixed λ and n. $n = 1$ corresponds to symmetrical solution. $\lambda = 0$; $d = 5\,\mu$m; $l/d = 200$; $l_s/l = 2{\cdot}5$; $d_s/d = 5$; $\bar{U} = 10$ m/s; $R = 1{\cdot}5$, giving $\langle\bar{\xi}\rangle = 72$; $\tau_s = 0{\cdot}036$; $\tau = 0{\cdot}039$. K_0 taken to be 50.

This equation was used to give an idea of K_0 values but should be treated with caution. Stubs sometimes have tapers and the dissimilar metallic interfaces may upset the effective values of material properties. From the static-temperature data of Champagne *et al.* (1969) one can deduce that K_0 varied between 30 and 60 for their probes. It can be seen that the shapes of the contours are affected by K_0 but the magnitudes of the ϵ's are much the same. Also shown in figure 8 are the derivatives $(\partial q/\partial\lambda)_0$, $(\partial q/\partial n)_0$ and $(\partial q/\partial\xi_1)_0$. These are not significantly affected by the value of K_0. The only missing data are the unknown derivatives $(d\lambda/dU)_0$, $(dn/dU)_0$ and $(d\xi_1/dU)_0$.

Now perturbations in λ, n and ξ_1 must be chosen such that $\langle\xi\rangle$ follows the usual approximate King's law as U is varied. This allows a variety of variations for λ, n and ξ_1 to simulate perturbations in the symmetry of wire cooling. It is difficult to know how to vary λ, n and ξ_1 but reasonable guesses can be made by observing how hot spots move about. See, for example, figures 7 (b, c). The authors contend at this stage that weighting factors of equal order ($\simeq\frac{1}{3}$) in (17) are reasonable. Errors of $\epsilon \approx 10\,\%$ or higher are quite plausible.

In spite of the missing information, definite conclusions can be reached. If perturbations in λ alone occur, then ϵ_λ is the appropriate step in response and similarly for perturbations in the quantities n and ξ_1. These conclusions follow directly from the well-accepted basic equation (8) and the rigorously derived end conditions. No approximations have been made other than the asymptotically exact linearizing approximations. For higher resistance ratios, the errors increased in some cases and decreased in others.

To find the order of the frequency range of the step one must determine the full frequency-dependent solution of (11). This has been done for perturbations in ξ_1. Perturbations in other quantities have not been attempted. Figure 9 shows some typical

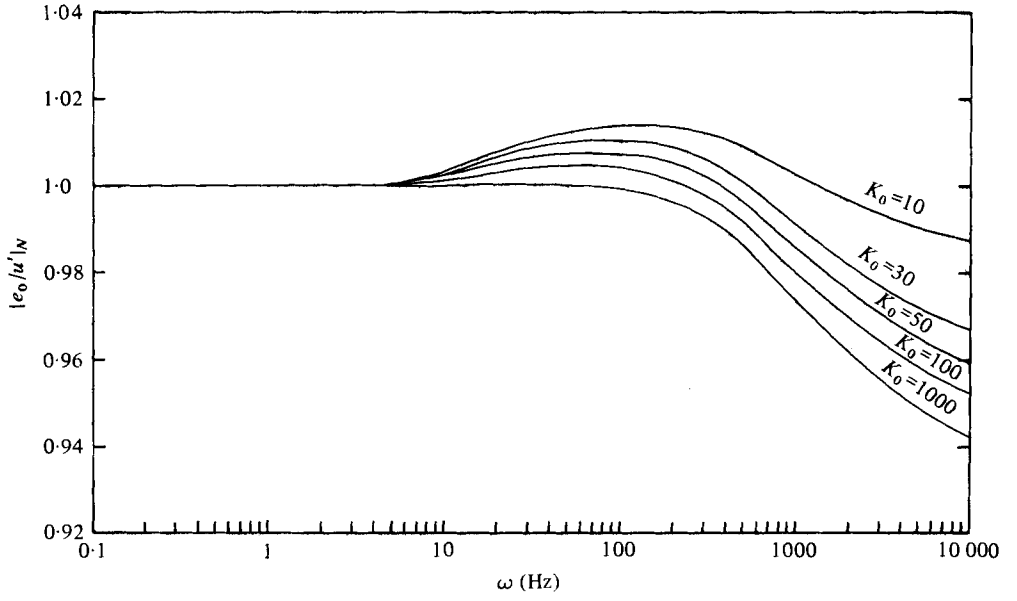

FIGURE 10. Theoretical Bode plots for symmetrical wires for different values of K_0. $\lambda = 0$; $n = 1$; $\langle\bar{\xi}\rangle = 72$; $\tau_s = 0{\cdot}036$; $\tau = 0{\cdot}039$; $R = 1{\cdot}5$.

frequency response curves. Calculated values of e_{ξ_1}, from the full solution, were found to agree with the earlier asymptotic calculations. It can be seen that, the more asymmetrical ξ is, the more the effects of the wire merge with the effects of the stub.

4.3. *Simple symmetrical solutions*

For the simple case of uniform ξ, all boundary conditions are symmetrical and a simple analytical solution can be obtained for the case of negligible wire time constant:

$$\left(\frac{e_0}{u'}\right)_N = 1+\epsilon\frac{(\tau_s s)^{\frac{1}{2}}\coth(\tau_s s)-1}{(\tau_s s)^{\frac{1}{2}}\coth(\tau_s s)^{\frac{1}{2}}}, \tag{26}$$

where
$$\epsilon \approx 1/RK_0 \tag{27}$$

for
$$K_0 \gtrsim 20.$$

For the case of a negligible stub effect and for sufficiently high frequencies the solution is

$$\left(\frac{e_0}{u'}\right)_N = \left[1-\frac{2}{\overline{\Pi}^{\frac{1}{2}}}\left(\frac{1}{p}+\frac{p}{p+1}\right)\right]\Big/\left[1-\frac{2}{\overline{\Pi}^{\frac{1}{2}}}\left(\frac{1}{p}+\frac{\bar{q}}{\bar{\xi}}\frac{p}{p+1}\right)\right], \tag{28}$$

where $p = (1+T_w s)^{\frac{1}{2}}$, in which $T_w = \tau/\overline{\Pi}$ and $\overline{\Pi} = \bar{\xi}-\bar{q}$. This gives a step in frequency response

$$\epsilon = -1/\overline{\Pi}^{\frac{1}{2}}R. \tag{29}$$

These symmetrical solutions are shown in figure 10 for different values of K_0. Equation (28) was first arrived at by de Haan (1971).

5. Conclusions and discussion

In the case of temperature-fluctuation measurements, the theory and experiment agree reasonably well. Significant steps in frequency response occur with a centre-frequency of about $\frac{1}{8}$ Hz. The step is as large as 30 % for an l/d ratio of 100 and decreases for increasing l/d. The problem appears to be relatively straightforward and the step size can be calculated from a very simple formula. The step in response spans approximately a decade.

In the case of velocity-fluctuation measurements, the problem is intractable since it depends on quantities over which one has little control. A high resistance ratio causes the wire to bow owing to thermal expansion, and aeroelastic effects enter the problem; in general there appears to be a lack of symmetry in temperature distributions. By perturbing the spatial mean film coefficient according to the usual heat-transfer laws and in addition perturbing its symmetry, one finds that significant errors are possible. Furthermore, phenomena within the wire usually associated with high-frequency behaviour extend their influence down to low frequency.

Differences in frequency response between wires have been observed to be as large as 10 % or higher (or 20 % in mean-square energy).

The frequencies of a given step can range from about 10 Hz to 1 kHz or more. Unlike the temperature-measuring case, where bulk heating of the prong occurs, lumped systems must be replaced by distributed systems. The lack of wire symmetry apparently causes heat waves to travel along the wire, thus reducing its effective time constant. From tests carried out this appreciable step in the response can occur with all wire geometries, resistance ratios and mean velocities.

If precise measurements of turbulence are required, e.g. for establishing similarity laws based on absolute velocity scales such as the friction velocity in pipe or boundary-layer flows, it seems that wires should be calibrated dynamically at frequencies of the order of the turbulence being measured. Perhaps a scheme using turbulence from a standard grid could be devised.† Until such a scheme is developed, the only practical solution is to repeat the required measurements a number of times using different wires.

The authors wish to acknowledge the financial support of the Australian Research Grants Committee, the Australian Institute of Nuclear Science and Engineering and the U.S. Navy, ONR – Contract No. N0014-67-A-0037 Task NR062-431. Some of this work was done in co-operation with G.A.L.C.I.T. The valuable experimental assistance of Dr P. H. Hoffmann and Mr S. Henbest of the Department of Mechanical Engineering, University of Melbourne, is also acknowledged.

† Suggested by a colleague: Dr C. A. Abell of the University of Adelaide.

REFERENCES

BETCHOV, R. 1948 *Proc. Ned. Akad. Wetenschappen* **51**, 721.
CHAMPAGNE, F. H., SLEICHER, C. A. & WEHRMANN, O. H. 1967 *J. Fluid Mech.* **28**, 153–175.
HAAN, R. E. DE 1971 *Appl. Sci. Res.* **24**, 231.
HINZE, J. O. 1959 *Turbulence*, chap. 2. McGraw-Hill.
MAYE, J. P. 1970 *DISA Inf.* no. 9.
PERRY, A. E. 1972 *J. Sound Vib.* **22**, 41.
PERRY, A. E. & MORRISON, G. L. 1971*a* *J. Fluid Mech.* **47**, 765.
PERRY, A. E. & MORRISON, G. L. 1971*b* *J. Fluid Mech.* **50**, 815.
PERRY, A. E. & MORRISON, G. L. 1972 *J. Phys.* E **5**, 1004.

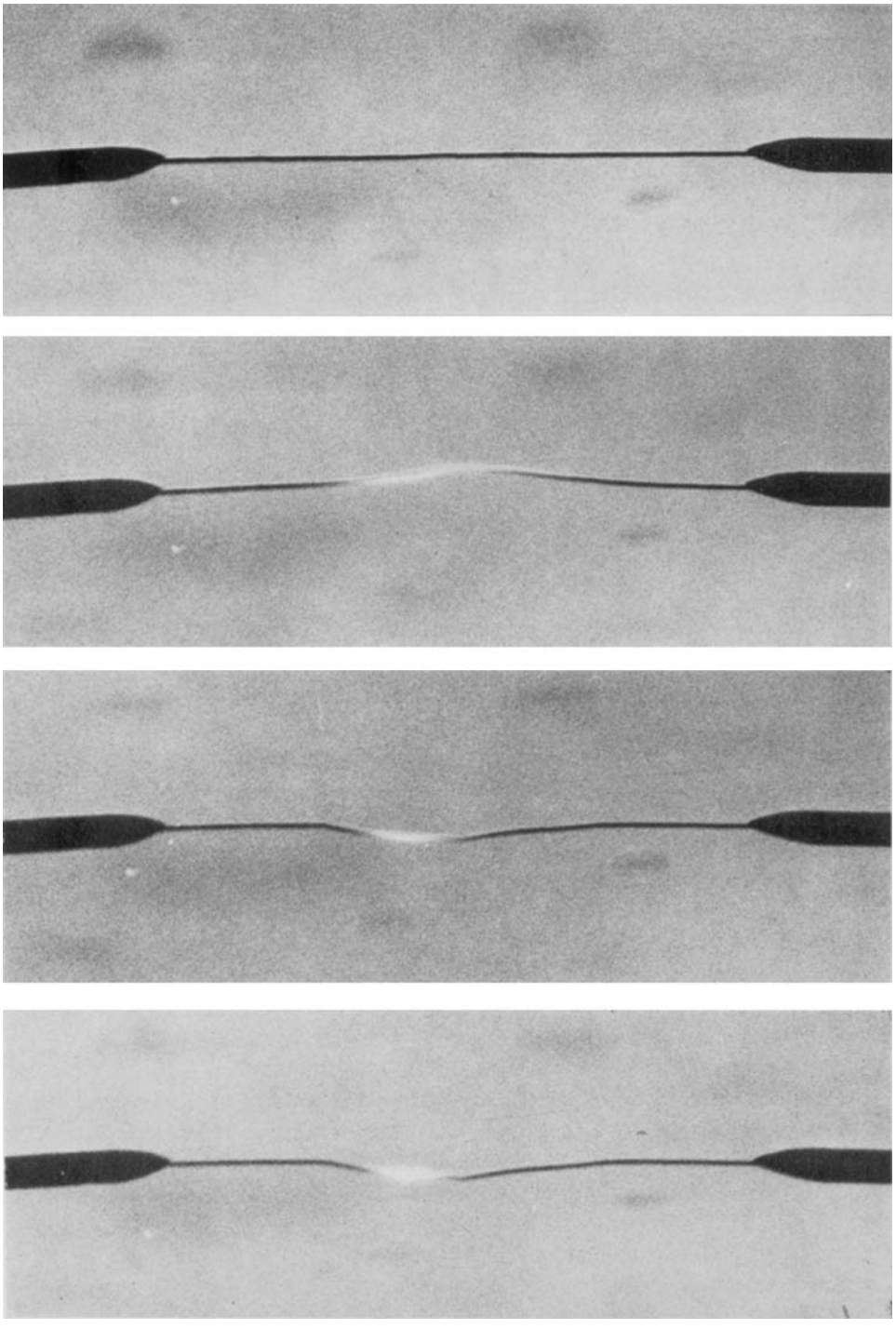

FIGURE 6. Observation of hot spots. (*a*) Straight wire with no current, $l/d = 100$. (*b*) With current flowing through wire, $R \simeq 2{\cdot}5$. (*c*) Same wire with air flowing downwards (10 m/s). (*d*) Same wire with higher air flow (20 m/s). Hot spot enhanced by multiple exposure.